IOPscience iopscience.iop.org

Home Search Collections Journals About Contact us My IOPscience

A micro-scale printable nanoclip for electrical stimulation and recording in small nerves

This content has been downloaded from IOPscience. Please scroll down to see the full text.

2017 J. Neural Eng. 14 036006

(http://iopscience.iop.org/1741-2552/14/3/036006)

View the table of contents for this issue, or go to the journal homepage for more

Download details:

IP Address: 168.122.66.3
This content was downloaded on 27/07/2017 at 03:27

Please note that terms and conditions apply.

You may also be interested in:

Rodent model for assessing the long term safety and performance of peripheral nerve recording electrodes
Srikanth Vasudevan, Kunal Patel and Cristin Welle

The design of and chronic tissue response to a composite nerve electrode with patterned stiffness
M J Freeberg, M A Stone, R J Triolo et al.

Functional recordings from awake, behaving rodents through a microchannel based regenerative neural interface
Russell K Gore, Yoonsu Choi, Ravi Bellamkonda et al.

Recording nerve signals in canine sciatic nerves with a flexible penetrating microelectrode array
Donghak Byun, Sung-Joon Cho, Byeong Han Lee et al.

High-resolution measurement of electrically-evoked vagus nerve activity in the anesthetized dog
Paul B Yoo, Nathan B Lubock, Juan G Hincapie et al.

Clinical applications of penetrating neural interfaces and Utah electrode array technologies
Richard A Normann and Eduardo Fernandez

Fascicular nerve stimulation and recording using a novel double-aisle regenerative electrode
I Delgado-Martínez, M Righi, D Santos et al.

IMT SCHOOL FOR ADVANCED STUDIES LUCCA
2017/18 PhD program at
IMT School for Advanced Studies Lucca
Deadline for applications – July 31st 2017, 6 pm Italian time

IOP Publishing Journal of Neural Engineering

J. Neural Eng. **14** (2017) 036006 (11pp) https://doi.org/10.1088/1741-2552/aa5a5b

A micro-scale printable nanoclip for electrical stimulation and recording in small nerves

Charles A Lissandrello[1,7], Winthrop F Gillis[2,7], Jun Shen[2], Ben W Pearre[2], Flavia Vitale[3,6], Matteo Pasquali[3,4], Bradley J Holinski[5], Daniel J Chew[5], Alice E White[1] and Timothy J Gardner[2,8]

[1] Department of Mechanical Engineering, Division of Materials Science and Engineering, and the Photonics Center, Boston University, Boston, MA 02215, United States of America
[2] Department of Biology and Department of Biomedical Engineering, Boston University, Boston, MA 02215, United States of America
[3] Department of Chemical and Biomolecular Engineering, Rice University, Houston, TX 77005, United States of America
[4] Department of Chemistry, Rice University, Houston, TX 77005, United States of America
[5] GlaxoSmithKline, Bioelectronics R&D, Stevenage, Hertfordshire, United Kingdom
[6] Current address: Department of Neurology, Center for Neuroengineering and Therapeutics, University of Pennsylvania, Philadelphia, PA 19104, United States of America

E-mail: timothyg@bu.edu

Received 27 October 2016, revised 19 December 2016
Accepted for publication 19 January 2017
Published 21 March 2017

Abstract

Objective. The vision of bioelectronic medicine is to treat disease by modulating the signaling of visceral nerves near various end organs. In small animal models, the nerves of interest can have small diameters and limited surgical access. New high-resolution methods for building nerve interfaces are desirable. In this study, we present a novel nerve interface and demonstrate its use for stimulation and recording in small nerves. *Approach*. We design and fabricate micro-scale electrode-laden nanoclips capable of interfacing with nerves as small as 50 μm in diameter. The nanoclips are fabricated using a direct laser writing technique with a resolution of 200 nm. The resolution of the printing process allows for incorporation of a number of innovations such as trapdoors to secure the device to the nerve, and quick-release mounts that facilitate keyhole surgery, obviating the need for forceps. The nanoclip can be built around various electrode materials; here we use carbon nanotube fibers for minimally invasive tethering. *Main results*. We present data from stimulation-evoked responses of the tracheal syringeal (hypoglossal) nerve of the zebra finch, as well as quantification of nerve functionality at various time points post implant, demonstrating that the nanoclip is compatible with healthy nerve activity over sub-chronic timescales. *Significance.* Our nerve interface addresses key challenges in interfacing with small nerves in the peripheral nervous system. Its small size, ability to remain on the nerve over sub-chronic timescales, and ease of implantation, make it a promising tool for future use in the treatment of disease.

Keywords: cuff electrode, nerve cuff, 3D printing, microelectrode

(Some figures may appear in colour only in the online journal)

[7] Charles Lissandrello and Winthrop Gillis contributed equally to this work.
[8] Author to whom any correspondence should be addressed.

 © 2017 IOP Publishing Ltd Printed in the UK

1. Introduction

There is growing evidence that many chronic diseases can be treated through modulation of the peripheral nervous system (PNS). Positive clinical trials can be found for vagal nerve stimulation to treat inflammatory diseases (Koopman 2016) as well as vagal nerve stimulation to treat depression and epilepsy (Tarver and Cummins 2006, Morris 2013, Moore 2015). Looking beyond these first results, it is thought that a broad range of diseases such as diabetes, polycystic ovarian syndrome, asthma, and cancer may be treatable through modulation of the autonomic nervous system, either by electrically blocking or stimulating the nerve to modify organs directly, or to modify the brain's reflex control of the organs indirectly (Famm 2013). Current nerve interfaces typically consist of two or more electrodes and a supporting structure that maintains these electrodes in contact with a peripheral nerve to stimulate or record neural activity.

The vagus nerve, which has been the target of previous clinical studies, contains numerous fascicles that innervate a variety of organs, and bulk stimulation of the vagus nerve is often accompanied by non-specific effects resulting from stimulation of axons unrelated to the target (Sackeim 2001, Koopman 2016). Fortunately, the anatomical organization of the PNS can be exploited whereby functional branches diverge as they near their target organ. It is at these distal branches where organ modulation can be more specific, avoiding off-target effects. Near the end organ, target nerves can be very small; for example, the carotid sinus nerve is only 300–400 μm in diameter, and is an important target for possible treatment of hypertension (Bakris *et al* 2012, Hoppe 2012) and diabetes (Conde 2014). In the mouse the carotid sinus nerve is only 50 μm in diameter, with no current technology option for interfacing and testing proof-of-principle for therapy. To advance basic research in bioelectronic medicine, for many targets in pre-clinical models, new miniaturized devices will be necessary (Famm 2013). Recent work has pushed the limits of electrode design to enable interfacing with nerves of diameters as small as 100 μm (Delivopoulos 2012). There are also now commercially available cuff electrodes at sizes down to 100 μm (CorTec GmbH, Freiburg, Germany). However, the manual fabrication process for these small electrodes limits the consistency of their geometry, leading to variability of performance. For cuff electrodes targeting the smallest nerves, the inner diameter may be 100 μm, but the outer diameter is often much larger, leading to tight geometries for nerves with small, deep access points in the body, such as the carotid sinus nerve.

Since many nerves of interest are located away from any support bone structure, they are also exposed to continuous movement in the viscera. For the smallest nerves, we postulate that carbon nanotube fibers (CNTfs) could provide good electrical impedance (Vitale 2015) but also favorable mechanical properties including minimal tethering forces due to their small diameter and stiffness. The CNTfs used in this study have a diameter of 12 μm and Young's modulus of 186 GPa (for comparison, the Young's modulus of 70/30 Platinum Iridium alloy is 236 GPa). While the present study does not include chronic recording or stimulation, we describe a device built around CNTfs in anticipation of future chronic recording and stimulation tests.

In order to secure existing cuff electrodes around the nerve, they are usually sutured closed (MicroProbes, Gaithersburg, MD), or employ closure mechanisms such as buckles (CorTec GmbH, Freiburg, Germany). In all cases, these devices require micromanipulation with forceps, requiring significant expertise. The goal of rapid keyhole surgery is challenging or impossible with existing designs. Biocompatible glues like fibrin sealants (Baxter International Inc.) can also be used to cover the cuff and nerve to provide mechanical stability until connective tissue growth permanently secures the cuff. Nevertheless, existing closure mechanisms are often prone to failure and nerve devices frequently dislodge from the nerve after implant.

To recapitulate, in order to reliably interface with the small visceral nerves there are three hurdles that must be addressed: (1) small size, (2) ability to withstand motion without dislodging from the nerve and (3) ease of implantation/one handed manipulation. Here, we present a compact and flexible nerve nanoclip which addresses these key challenges through rapid fabrication at small sizes ($<1\,\mathrm{mm}^3$) using a direct-write 3D lithography technique, and a trapdoor geometry that allows for irreversible, forceps-free application of the device to the nerve.

Our approach leverages several technological advancements in order to produce novel, integrated micro-scale nerve nanoclips. The nanoclips were fabricated using the *Nanoscribe Photonic Professional GT* two-photon direct-write 3D lithography system (Nanoscribe GmbH, Germany) with a resolution of 200 nm. This system has been used by others to fabricate a myriad of micro-scale devices, including photonic structures (Atwater 2011), microfluidics (Hu 2014), and mechanical metamaterials (Bückmann 2012), but to our knowledge, our work is the first to use this technology to create integrated and implantable systems. The nanoclip presented here was fabricated from a commercially available, UV-curable polymer (*IP-Dip*, Nanoscribe GmbH, Germany) which has been shown to have a Young's modulus of $E \approx 1$ GPa (Bückmann 2014). This material selection allowed for the fabrication of flexible parts with proper geometric design, but other UV-curable polymers can be used for further design flexibility. Another innovation is the integration of CNTfs for use as robust, flexible electrodes. Because of these advancements, our fabrication platform is extremely versatile in the dimensions and geometric complexity of the nanoclips that can be produced, and in the type and number of electrodes that can be incorporated. The system allowed for a rapid experimentation cycle with design, printing, and implantation all possible within 2–3 d. Fine details of the design such as dimensions and flexibility were tuned to develop a nanoclip that was compact, easy to handle and implant, and able to irreversibly latch around the nerve without restricting normal nerve signaling. The nerve cuff described here is printed in sub-micron resolution, and for this reason we refer to the device as a 'nanoclip'.

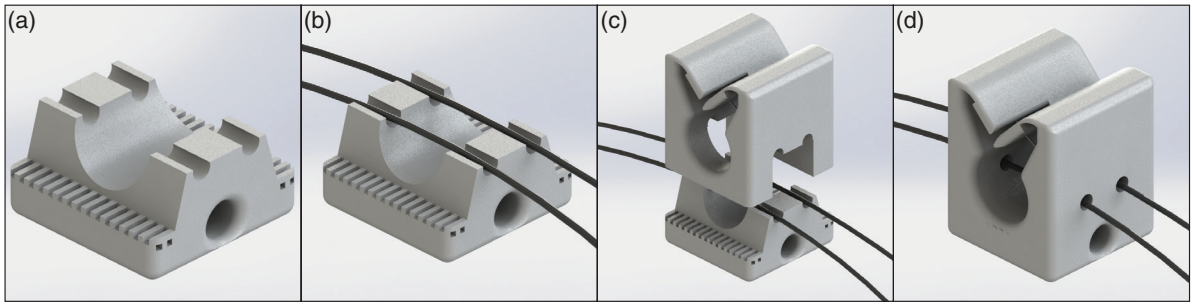

Figure 1. Illustration of nanoclip printing process. (a) The base of the nanoclip is printed. (b) A three-axis stage and dissection microscope are used to carefully align and place two CNTfs into the alignment slots. (c) After optical alignment, the top half of the nanoclip is printed. (d) The completed two-channel device.

2. Methods

2.1. Nanoclip fabrication

The nanoclips were designed and modeled using solid-modeling software (*SolidWorks*, Daussalt Systèmes SolidWorks Corporation, Waltham, MA) and finite element analysis software (*COMSOL Multiphysics*, COMSOL Inc., Burlington, MA). The design can be easily scaled and modified to accommodate various nerve sizes and geometries. Once a design was chosen, the nanoclips were then fabricated using the *Nanoscribe* lithography system. The system scanned a focused laser beam ($\lambda = 780$ nm) into a droplet of the commercially available, UV-curable polymer, *IP-Dip*. Galvanometer scanning mirrors controlled the position of the focal point in the writing plane and a piezo actuator moved the stage along the optical axis to write subsequent layers. Final structures were printed using a 50 mm s^{-1} linear scan speed and with the optical power set to 65% of maximum (~120 mW average power). These parameters allowed for the construction of devices with features as small as 200 nm over a writing area of ~300 μm in each dimension.

The fabrication was a multi-step process that required the base of the nanoclip to be fabricated, followed by manual placement of CNTf conducting electrodes, and subsequent fabrication of the upper half of the nanoclip, as illustrated in figure 1. First, the base of the nanoclip was fabricated on a clean silicon substrate (although the selection of the substrate material is not critical) (figure 1(a)). Two 35 μm semi-cylindrical cut-outs with a separation of 150 μm were incorporated into the base to provide alignment for the placement of two conducting electrodes. The base had a roughened surface (cross-hatch design) that increased the surface area for better integration with the top of the nanoclip. Large vertical features near interfaces were constructed at a 15° angle to prevent shadowing that would reduce the integration during printing of the top section. The base also included a 60 μm diameter hole that was used to insert a fine wire for easy handling by the surgeon. After the printing process, the sample was submerged in a solvent (Propylene glycol methyl ether acetate, Sigma-Aldrich Co., St. Louis, MO) for 20 min to rinse away unpolymerized resist and finally rinsed in a mild solvent with low surface tension (*3M Novec 7100 Engineered Fluid*, 3M, St. Paul, MN).

CNTfs were used as a high-tensile strength and highly flexible electrode material (Behabtu 2013). The CNTfs were suspended across a 3D-printed fork, which was attached to a motorized three-axis stage (*3DMS*, Sutter Instrument, Novato, CA). A stereoscopic microscope was used to carefully align the CNTfs over the semi-cylindrical cut-outs and to monitor while the CNTfs were lowered into the nanoclip base to ensure they spanned the nanoclip opening (figure 1(b)). The CNTfs were held down using double-sided tape placed on the periphery of the substrate. The substrate was then loaded back into the lithography system for the fabrication of the top half of the nanoclip. After optical alignment, the print began within the cross-hatched section of the base (figure 1(c)). After the print was completed, the unpolymerized resist was washed away, as described above, leaving the completed nanoclip structure. The fully-printed CNTf-laden device was then removed from the substrate and used in surgery. The complete printing time was approximately 30 min per device and total manufacturing time (including processing and assembly) was about 90 min per device. Next generation printing processes now in development in the Gardner lab will reduce this print time to 30 s or less.

2.2. Latch mechanism

The nanoclip design was modified in an iterative process that gradually improved the ease of use and the mechanical stability on the nerve. Continual feedback between surgeon and fabricator facilitated a rapid improvement in design, allowing for design iterations on the time scale of days. Computer-generated models and scanning electron microscope (SEM) images of fabricated designs are shown in figure 2. Early designs consisted of fixed geometry, semi-cylinder devices which had small teeth to grip on the nerve and relied on the deformable nature of the nerve to slide between the teeth on initial implantation. This design was abandoned because the devices typically fell off the nerve within a few weeks of implantation. The next design included a hinged door that could be latched on top of the nerve (figure 2(b)). This design was functional but ultimately was abandoned since it required an additional manipulator (e.g. pair of forceps) to depress and latch the door. The final design, tested for this study, consisted of two 'trapdoors' with a semi-cylindrical interior channel (figure 2(a)). In order to fabricate these doors using

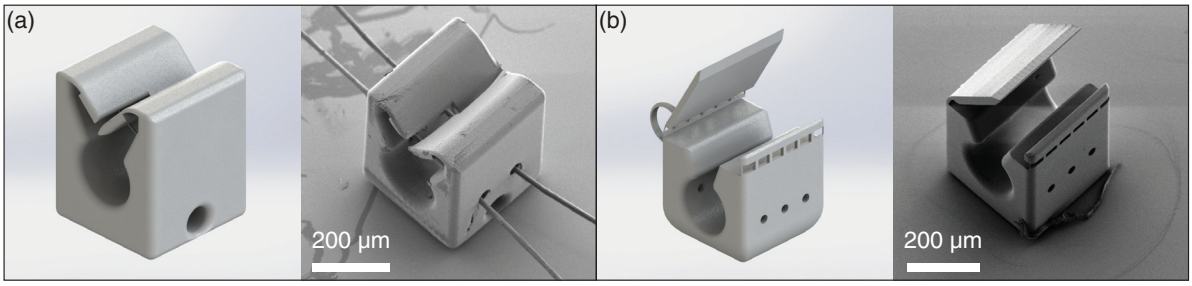

Figure 2. Evolution of nanoclip design. (a) A trap-door-type design with integrated CNTf electrodes and a through-hole for easy handling by the surgeon. A model, created in Solidworks, is shown on the left and a scanning electron microscope (SEM) image of a finished device is shown on the right. (b) Model (left) and SEM image (right) of a different design which utilizes a moveable, hinged door and includes three holes for CNTf integration.

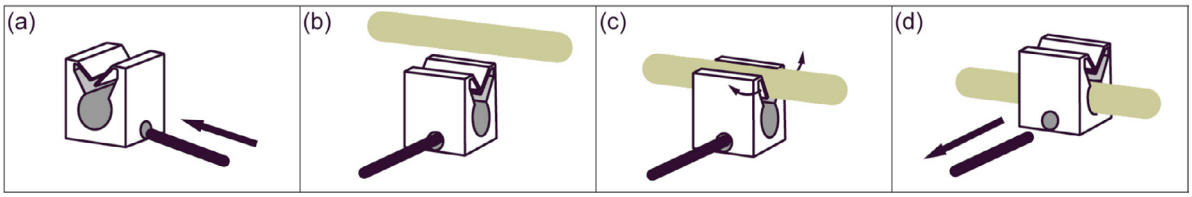

Figure 3. Illustration of the nanoclip implant process. (a) A fine wire (<60 μm) is inserted into the hole in the base. (b) The nanoclip is brought near an isolated TS nerve by the wire. (c) The nanoclip is pressed into the isolated nerve, causing the doors to open to allow entry of the nerve. (d) The doors close to secure the nanoclip on the nerve and the wire is removed from the base.

the 3D direct-write lithography system, small support rods were added to provide stability during the printing process. These support rods were engineered to bend out of the way during implantation but do not break off. The doors and support rods were tested by repeated bending cycles performed using a linear stage to advance a needle toward the cuff under a microscope. During implantation, the device was advanced towards the nerve eventually resulting in elastic deformation of the doors and subsequent entry of the nerve into the central channel (figures 3(a)–(c)). After the nerve cleared the doors, the doors would return to their original configuration, permanently locking the nerve inside (figure 3(d)). This design only required a single micromanipulator or hand-held manipulator (attached with a fine wire) to deliver the device, therefore, requiring a smaller incision. With this design, all devices remained on the nerve for the entirety of the sub-chronic tests described below.

2.3. Experimental protocol

Two experiments were performed with variations of the nanoclip: (1) evaluation of sub-chronic nerve damage due to implant (not electrically functional) (2) acute electrophysiology (uninsulated nanoclips). All surgical procedures were done in accordance with our IACUC approved protocol.

2.3.1. Evaluation of sub-chronic nanoclip safety based on song behavioral readouts (n = 4). Nanoclips manufactured without CNTfs (not electrically functional) were attached to the tracheal syringeal (TS) (hypoglossal) nerve of male zebra finches for sub-chronic evaluation of nerve health based on physiological readouts. For three implants, nanoclips were implanted on both the left and right TS nerve, and for one implant, a nanoclip was implanted unilaterally on the right TS nerve. The zebra finches were induced and maintained with 3% isoflurane/97% oxygen. The feathers on their neck and over the breast muscle were plucked to expose their skin. 120 μl of the analgesic Meloxicam was injected into the breast muscle to reduce pain and inflammation. The skin was then disinfected with 70% ethanol and betadine. A 1.5–2.0 cm incision was made in the skin of the right neck. Two sutures were attached to each side of the incision to keep the neck opened during the procedure. Fatty tissue was removed from the opening and the trachea was exposed. Next, connective tissue attaching the TS nerve was removed from a portion of the nerve near both the head and the body, about 8–10 mm apart from each other. A small piece of biocompatible vinyl tubing was placed underneath the nerve to temporarily isolate it from the body. The body cavity was moistened with a bath of phosphate-buffered saline (PBS). Finally, the nanoclip electrode was implanted on the nerve using the aforementioned procedure (figure 3). Optical microscope images of two different nanoclips, after attachment to the nerve, are shown in figure 4. We note that the blood vessel supplying the implanted nerve was dissected away, in order to isolate the nerve, leading to an acute damage phase that was not controlled for in these tests. This blood vessel removal was not required as part of the implant, and future studies will compare implants with and without local blood vessel dissection. Following the implant procedure, the zebra finches were sutured up and allowed to recover.

We compared nerve damage from bilateral nanoclip implantations to nerve damage from bilateral nerve crush procedures. To carry out the experiment, three zebra finches were induced using the procedure described above. Both the left and right nerve were exposed, isolated, and crushed at a width of ~300 μm to simulate the width of the nanoclip. The crush was applied at a similar location to the placement of the nanoclip. The zebra finches were sutured up and allowed to

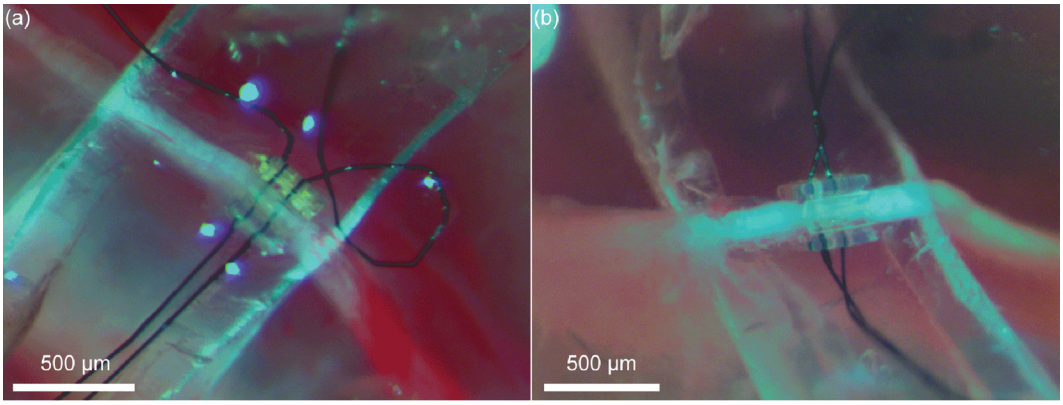

Figure 4. (a,b) White light images of CNTf-laden devices implanted on the tracheal syringeal nerve. The doors are observed to be closed around the nerve in (b).

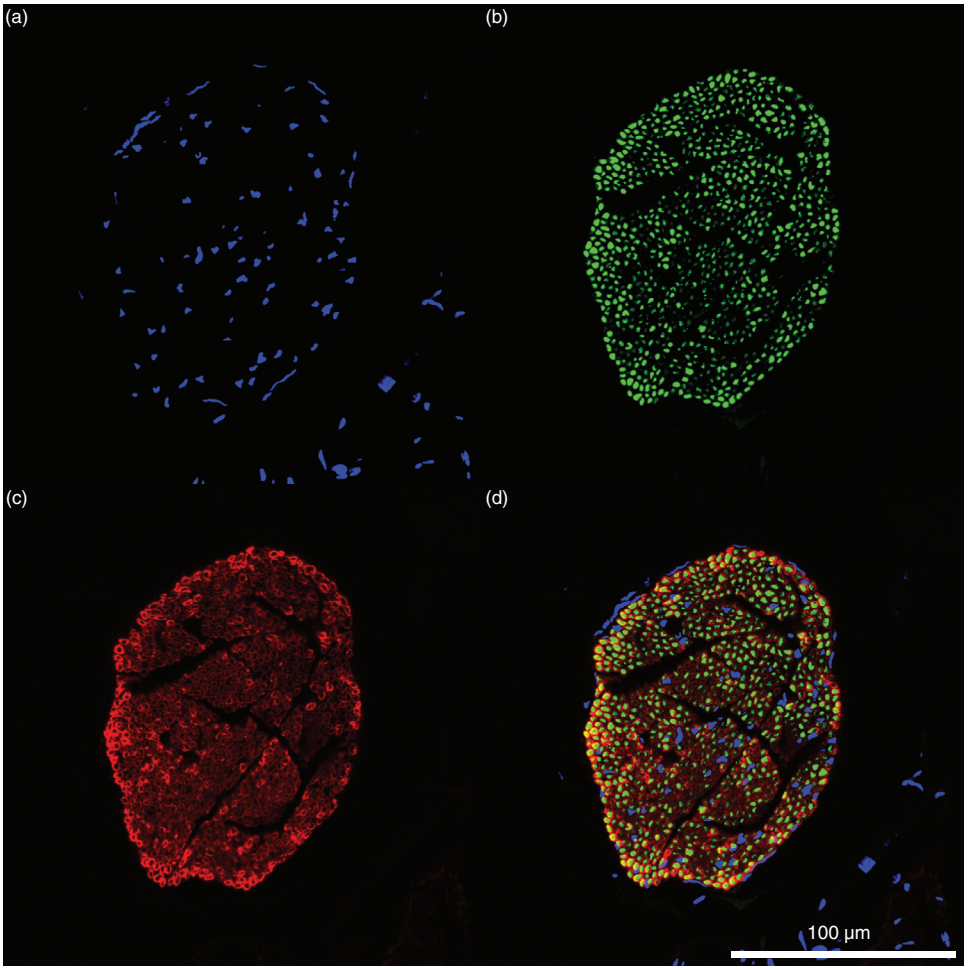

Figure 5. Immunohistochemistry of TS nerve cross-section. (a) DAPI stain, (b) anti-neurofilament (3A10) labelling, (c) anti-myelin basic protein (MBP) labelling, and (d) composite image. Myelin (red) is found surrounding 99% of the axons.

recover. A fourth zebra finch was left untouched and song was observed for 3 weeks as a negative control.

Birdsong was recorded daily and subtle changes from baseline song were a sensitive surrogate marker of neural damage. Audio recordings were made with a sampling rate of 48 kSa s^{-1} continuously throughout each day of study. These long recordings were analyzed to identify individual songs and days were disregarded if they did not contain more than ~50 identified songs. We quantified the change in birdsong by extracting important features of the spectrum (Poole 2012) and computing the Euclidean distance between feature sets. For further details, see 'Statistics'.

2.3.2. Histological definition of the TS nerve. We were unable to find a histological characterization of the TS nerve in zebra finches, and here report baseline histology of the TS nerve.

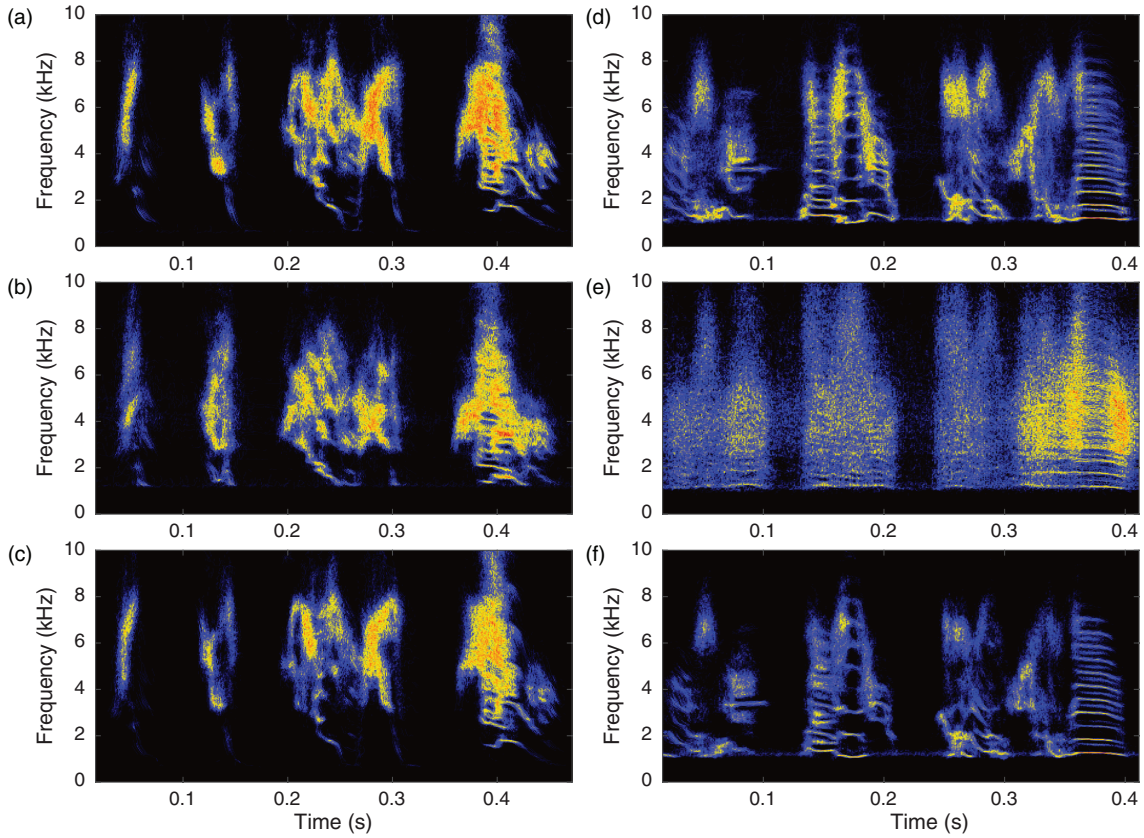

Figure 6. Song damage and recovery from a bilateral nanoclip implant (a)–(c) and bilateral nerve crush (d)–(f). Spectral density image of bird *lny31* birdsong (a) before surgery, (b) 3 d after surgery, and (c) 4 weeks after surgery for $n = 100$ trials. Spectral density image of bird *lno37rlg* birdsong (d) before surgery, (e) 3 d after surgery, and (f) 4 weeks after surgery for $n = 100$ trials. In this case, song is minimally disrupted immediately following surgery. In both nerve crush and nanoclip implant, song typically returns most of the way to baseline within 10 d.

Histological analysis was performed in a control bird which did not have a nanoclip implant and had not been manipulated in any other way. We found that 99% of the nerve fibers are myelinated, in a single fascicle as described below. The relative uniformity of axon type explains the simplicity of the compound action potential evoked in stimulation of the nerve. To perform this histology, a male zebra finch was euthanized with a lethal dose of pentobarbital (120 μl) and perfused intracardially with 0.1 M PBS followed by 4% paraformaldehyde in 0.1 M PBS. During perfusion, the bird's neck was stretched to straighten the nerve for sectioning. Baseline histology of the TS nerve lateral cross-section is shown in figure 5. The trachea was treated with increasing concentrations of sucrose overnight. A small segment, located in the middle of the nerve, was transversely sectioned in 30 μm segments. We used DAPI to stain cell nuclei (figure 5(a)), an anti-neurofilament antibody (3A10) to label axons (figure 5(b)), and an anti-myelin basic protein (MBP) antibody to label the myelin sheath surrounding the axons (figure 5(c)). The myelination of the nerve is apparent from the Red MBP staining, as shown in figure 5(c). The sections were imaged with an Olympus FV10i confocal microscope.

To determine the number of axons in the TS nerve cross-section, we used the anti-neurofilament stain. We adjusted the color saturation of the image to clearly demarcate axon boundaries. A researcher then counted the number of axons in the nerve based on the anti-neurofilament stain. To count the number of axons that did not have myelin surrounding them, we used both the anti-myelin and anti-neurofilament stains. The color saturation for the red and green channels (anti-myelin and anti-neurofilament, respectively) was adjusted to more easily compare axons. An axon was considered to be without myelin if there was not a visible myelin (red) ring around the neurofilament (green). These measurements were done using the ImageJ software package.

2.3.3. Acute electrophysiology in oil-insulated nanoclip electrodes ($n = 4$). Zebra finches were anesthetized and nanoclips were implanted with the same technique as described above (section 2.3.1). In all cases, the blood vessels at the implant site were dissected along with the nerve epineurium. Two electrically functional identical nanoclips were implanted on the right nerve: one used for stimulation (rostral) and one used for recording (caudal). After the nanoclips were placed onto the nerve, the free ends of the CNTfs were tied to each other respectively, and suspended in air. Then, any PBS that resided in the vinyl tube was removed with an absorbent sponge and replaced with mineral oil. This removed any possible conduction path other than where the CNTfs were touching the nerve.

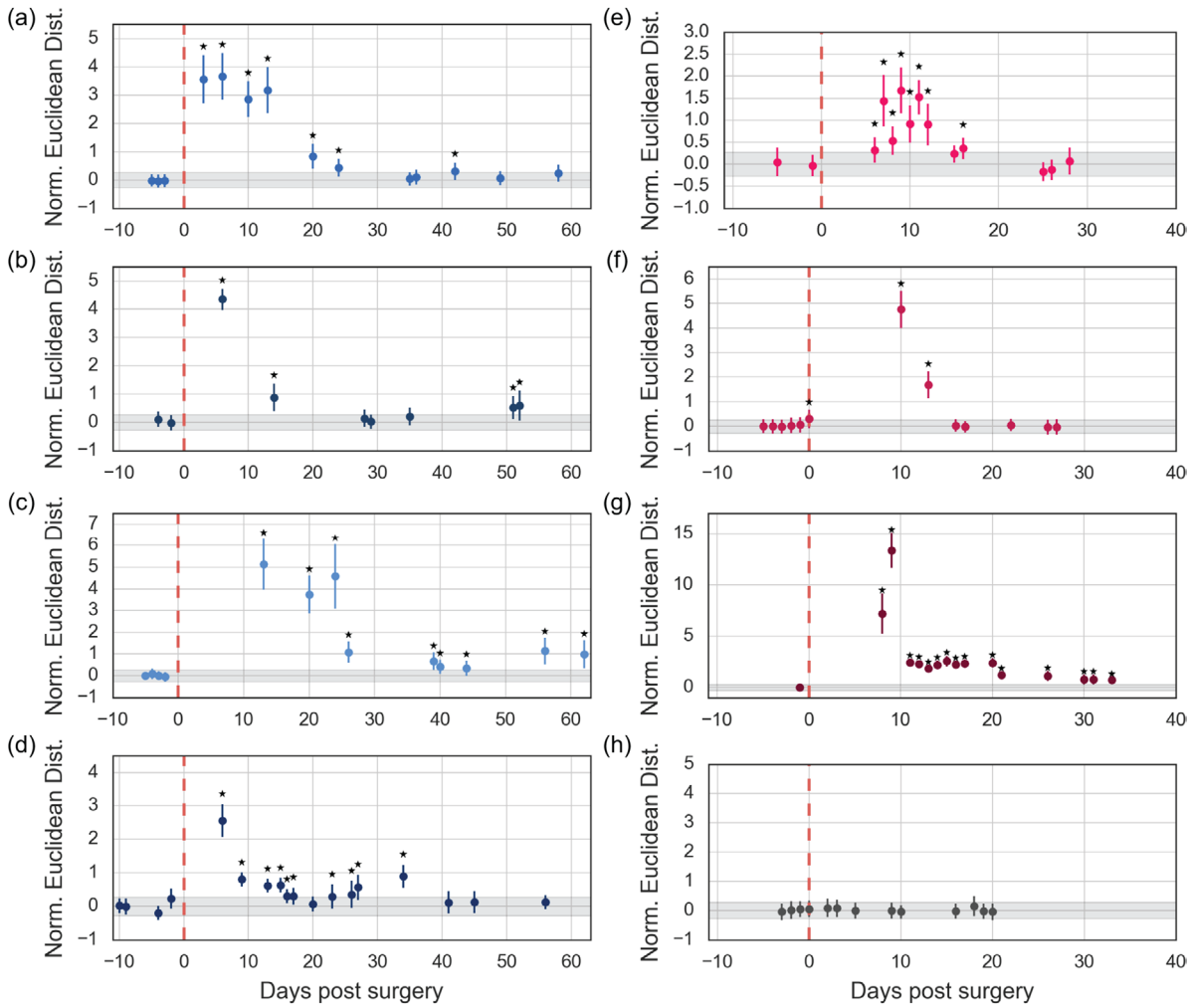

Figure 7. Comparison of zebra finch song recovery for nanoclip implant and nerve crush birds. Snug-fitting nanoclips were implanted bilaterally on birds (a) *lny29*, (b) *lny31*, and (c) *lny33*. A nanoclip was implanted unilaterally on bird (d) *lny37*. Bilateral nerve crushes were performed on birds (e) *lno37rlg*, (f) *lny71rb*, and (g) *lny76rb*. (h) Bird *lny88rb* served as a negative control, where birdsong was recorded in an untouched male. Normalized Euclidean distance between song features of 2 d of song. Each successive day is compared to a baseline day. Error bars represent one standard deviation. Stars indicate a song that has significantly deviated from baseline ($p < 0.0035$).

2.3.4. Stimulation and recording protocol. For electrophysiology experiments, two nanoclips, each containing two conducting electrodes, were placed on the nerve, separated by a distance of ~8–10 mm. The stimulation nanoclip (rostral) was connected to a PlexStim stimulator (*PlexStim*, Plexon Inc., Dallas, TX). The recording nanoclip (caudal) was connected to a TDT Medusa Preamplifier (*RA16PA*, Tucker-Davis Technologies, Alachua, FL). The recorded signal was band-pass filtered between 1 Hz and 20 kHz and sampled at 24 kSa s^{-1}. The nerve was subjected to a series of increasing amplitude biphasic current-controlled pulses until a response was seen on the recording electrodes. The stimulation threshold was recorded. Next, the amplitude was increased further, beyond the threshold value, and the nerve response activity was recorded. After stimulation-evoked responses were gathered, a small amount of bupivacaine, a sodium-channel blocker, was dripped onto the nerve at the stimulation site to prevent activation. This technique ensured that the evoked responses were neural and not due to signal contamination (e.g. electromyography artifact from neighboring muscles). We then repeated the stimulation to verify that the nerve activity was blocked at a range of currents. Following the procedure, the zebra finches were euthanized with sodium pentobarbital.

2.3.5. Statistics. Zebra finch song behavior provides an extremely sensitive and quantifiable readout of nerve damage. To test for differences in a bird's song across days, we measured the Euclidean distance between song features recorded from a baseline (pre-surgery) day to every other recorded day. Song features were computed for every aligned song, using a method reported previously (Poole 2012). Euclidean distance was calculated for every song combination between 2 d, for each recorded day.

To test for a significant change in song features shortly after surgery, a bootstrap was performed. The Euclidean spectral-feature distances for each recorded day was resampled 8000 times (85 data points, with replacement) and in each sampling, the median was calculated. This formed a Gaussian distribution of median values. This distribution was then normalized and compared to a similar distribution created from a negative control (no surgery). If the mean of a distribution was more

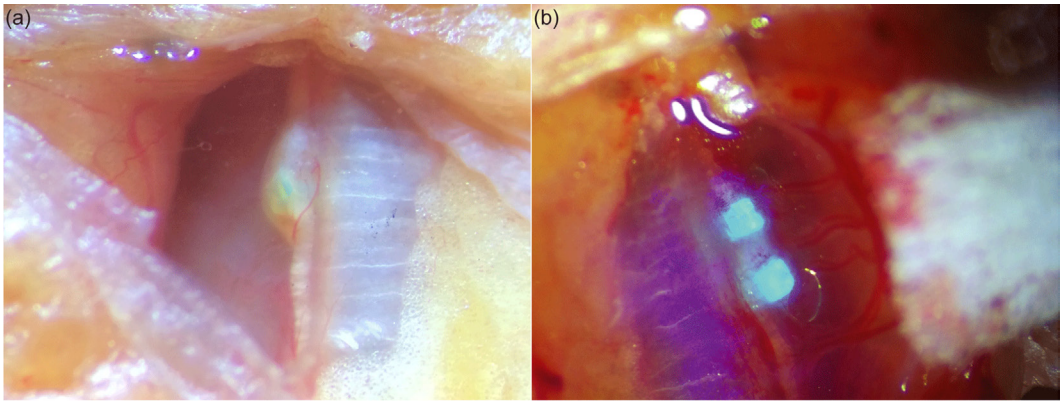

Figure 8. Visual inspection of sub-chronic implants. (a) White light image of a nanoclip implanted on a TS nerve (*lny37*) 74 d post-implant. (b) Example of two nanoclips (of an older design) under ultraviolet illumination 2 months post-implant. The upper nanoclip is seen attached to the nerve, while the lower nanoclip was not properly implanted onto the nerve and is observed to have come off. For scale, each nanoclip is approximately 300 microns on an edge.

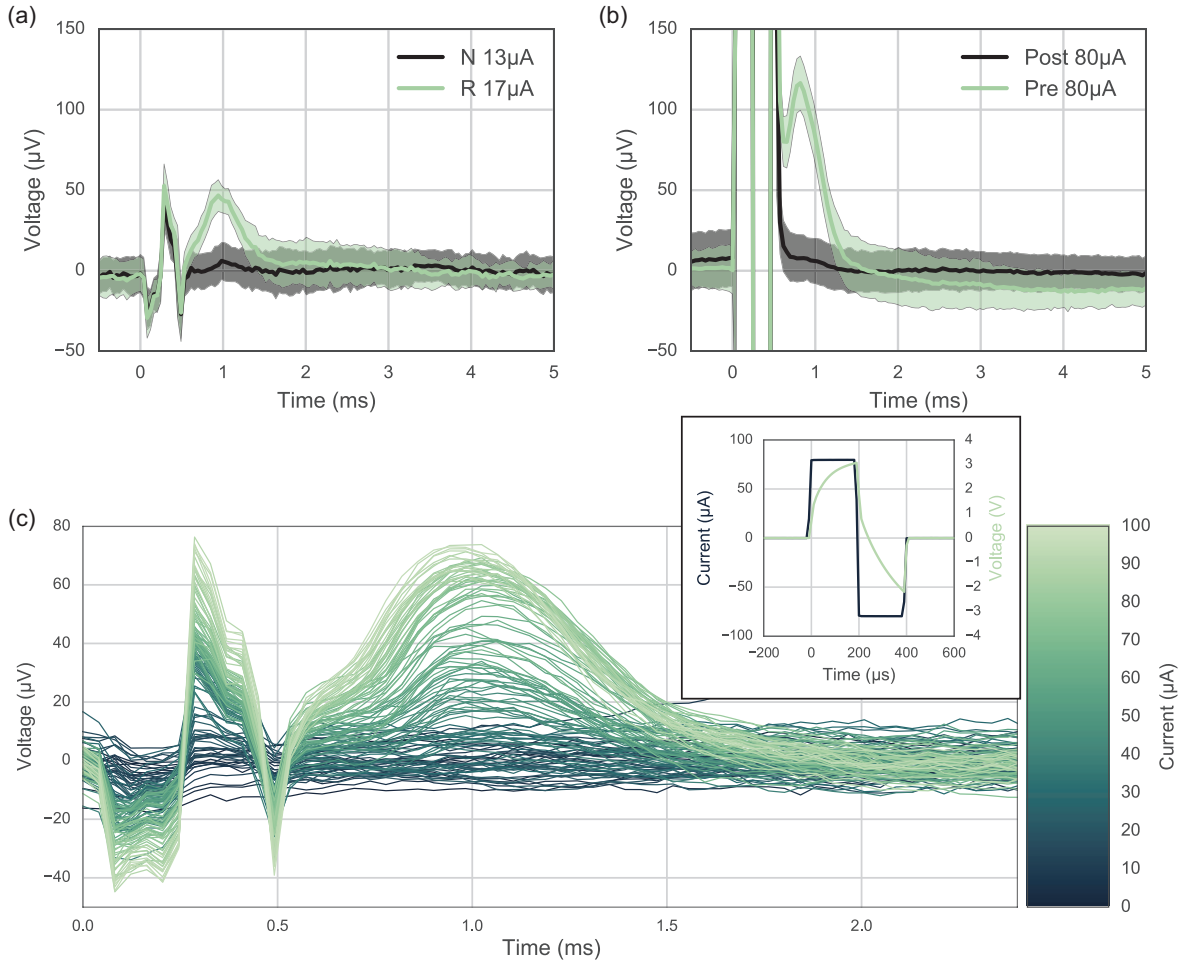

Figure 9. Stimulation-evoked response and stimulation thresholds. (a) Voltage response at sub-threshold and near-threshold current values. The downward spike at $t = 0$ is a stimulus artifact. (b) Voltage response before and after administering bupivacaine to block the nerve signal propagation. (c) Voltage response at increasing current values (ranging from $I = 1$–100 μA with 5% increments). Inset is the current and voltage of the stimulation waveform.

than three standard deviations away from the mean of the control distribution, that day was considered to be significantly different.

3. Results and discussion

3.1. Histological definition of the TS nerve

To understand the nerve's structural composition, we performed histological measurements of its cross section. Images taken from a single tissue segment of a control zebra finch (no nanoclip implant) are shown in figure 5. The results show that the nerve consists of a single fascicle of diameter 127.8 ± 17.4 μm ($n = 18$). It is also found that the majority of the axons within the nerve are myelinated and have an average diameter of 1.5 ± 0.6 μm. An average of $0.92\% \pm 0.42\%$ of axons within a nerve sample were unmyelinated, with an average of 1020 ± 126 axons per nerve ($n = 6$).

3.2. Evaluation of sub-chronic nanoclip safety based on song behavioral readouts

To evaluate the sub-chronic safety of the nanoclip, we attached non-electrically-functional nanoclips (without CNTfs) to the TS nerve of male zebra finches. Nanoclips were chosen from a range of sizes printed in 10 μm size intervals. The implanted nanoclip was chosen for a snug, but not tight fit, with complete closure of the hinges. We recorded and analyzed birdsong, as described above, to quantify neural damage. Birdsong spectral analysis is shown in figure 6 for a bilateral nanoclip implant (figures 6(a)–(c)) and a bilateral nerve crush (figures 6(d)–(f)) at multiple time points: before surgery, 3 d post-surgery, and 4 weeks post-surgery. Here, each plot contains the spectral density image (Poole 2012, see figure 3(a)) of aligned song ($n = 100$ trials), where color intensity indicates probability density. The song shows small deviations from the baseline song (figures 6(a) and (d)) 3 d post-implant (figures 6(b) and (e)), but recovers after 4 weeks (figures 6(c) and (f)).

The mean all-to-all Euclidean distance between song features is shown for eight individual birds in figure 7. Figures 7(a)–(c) are from bilaterally implanted nanoclips, figure 7(d) is from a unilaterally implanted nanoclip, figures 7(e)–(g) are from bilateral nerve crushes, and figure 7(h) is from a negative control, where the zebra finch was left untouched. In all cases, except the negative control, we observe disruption of the song immediately following surgery (as indicated by the red dashed line in the figure; $p < 0.0035$ bootstrap). In the weeks following surgery we observe a gradual return toward the baseline state, indicating healthy recovery of the nerve. One bird with a nanoclip implant (figure 7(c), *lny33*) and one bird with a nerve crush (figure 7(g), *lny76rb*), however, do not show complete recovery to baseline in this timeframe ($p < 0.0035$ bootstrap). It should be noted that blood vessels were dissected in the proximity of the nerve for the nanoclip implant surgeries (figures 7(a)–(d)); an unknown portion of the acute damage and recovery can be attributed to the loss and recovery of local blood supply.

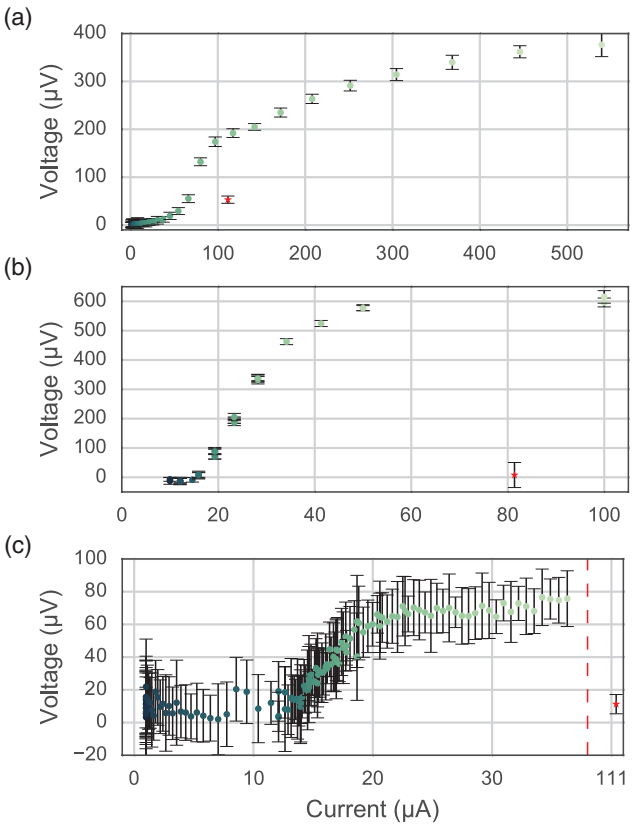

Figure 10. Maximum voltage of recruited compound action potentials as a function of stimulation current for birds (a) *lw7*, (b) *lw10*, and (c) *lw12*. Red stars indicate measurements taken after administering bupivacaine. Error bars represent one standard deviation. Note that axis scales are different for each panel.

The bilateral sub-chronic implants reveal that nerve functionality as measured by vocal performance returns to the baseline state in most cases. To confirm that the implanted nanoclips remained on the nerve, birds were sacrificed and the nerve-nanoclip visually inspected. The inspection process was aided by the fact that the polymer material used to fabricate the nanoclip is fluorescent under ultraviolet illumination. An optical microscope image of one nanoclip which had been implanted unilaterally (*lny37*) is shown 74 d post-surgery in figure 8(a). Two nanoclips (of an older design without trapdoors) are shown implanted on the TS nerve, under ultraviolet illumination, in figure 8(b). It should be noted that early designs were sometimes damaged during handling and were not always secured properly on the nerve in the first place. After many iterative rounds of improving upon the cuff geometry we were able to develop a design (figure 2(a)) which was more robust and was never found to come off the nerve in any of our experiments. In post mortem examination (see figure 8(a)), all nanoclips with our optimized geometry were found to be still latched over the nerve, with minimal qualitative evidence of local inflammation (no redness or swelling observed). In some cases, blood vessels were observed to have regrown around the outside of the nanoclip (figure 8(a)). These blood vessels were presumably newly grown to replace those which were dissected prior to implant.

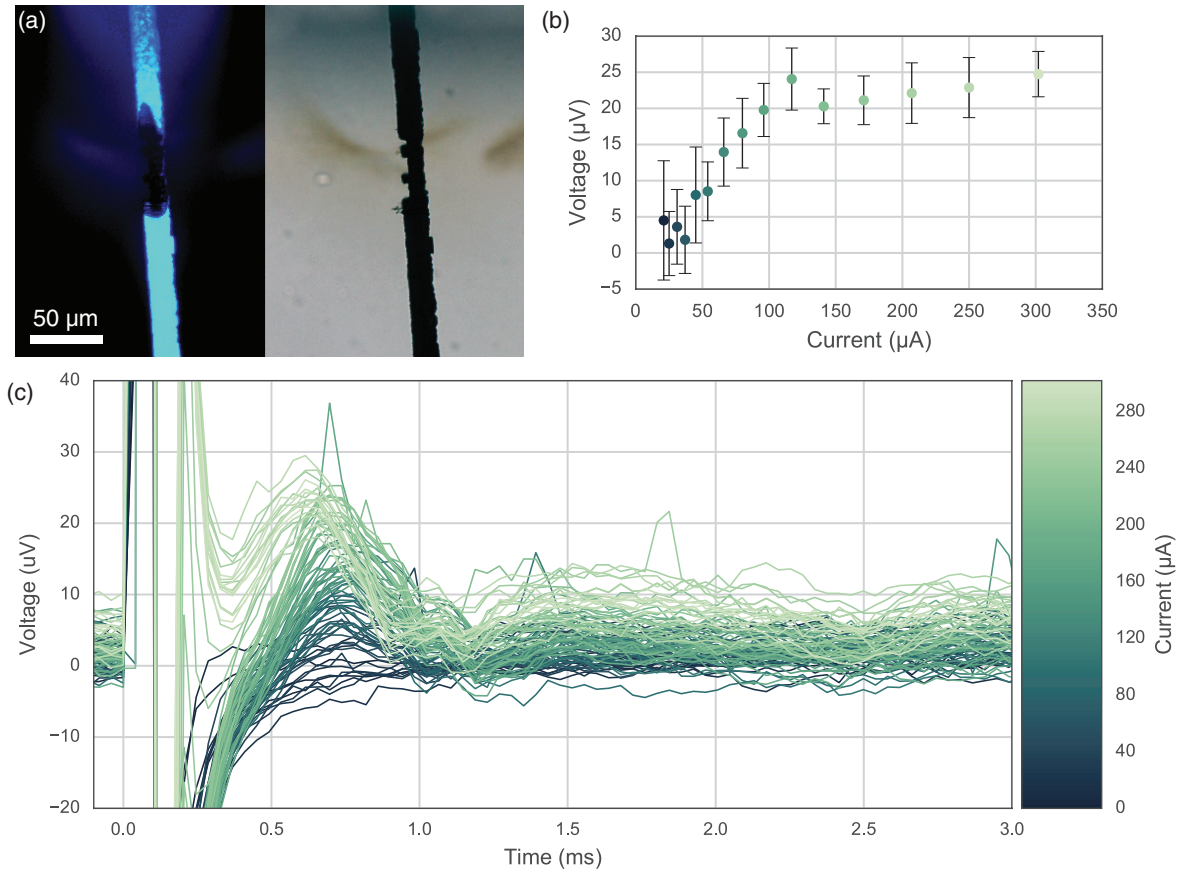

Figure 11. Demonstration of nanoclip electrodes with insulated CNTfs. (a) Optical images of parlyene-coated and laser-ablated CNTf viewed under ultraviolet (left) and white-light (right) illumination. (b) Maximum voltage of recruited compound action potentials as a function of stimulation current. Error bars represent one standard deviation. (c) Voltage response at increasing current values.

3.3. Acute electrophysiology in oil-insulated nanoclip electrodes

The stimulation-evoked response and stimulation threshold for one bird is shown in figure 9. Here, two electrically functional nanoclips were implanted on the right nerve for stimulation and recording, as described above. In figure 9(a), the voltage response measured at the recording nanoclip is shown for current values just below the stimulation threshold ($I = 13$ μA) and just above the threshold ($I = 17$ μA). Stimulation onset begins at $t = 0$ ms. Voltage deflections from the mean observed in the range $0 > t > 0.5$ ms are an artifact of the stimulus while the voltage deflections near $t = 1$ ms are the physiological response of the nerve. The voltage response at increasingly large current values is shown in figure 9(c) and an example stimulation waveform is shown inset. For this measurement, we vary the stimulation current in the range $I = 1$–100 μA, increasing in 5% increments. We observe an increase in the maximum physiological response voltage as we increase the stimulation current. Finally, we administer bupivacaine to block the nerve signal propagation, and observe cessation of the physiological response. In figure 9(b), we show the stimulation-evoked response for a current value well above stimulation threshold before and shortly after administering bupivacaine. Experiments of this type were repeated for multiple birds. In figure 10, we plot the peak response voltage of the measured signal as a function of stimulation current for three individual birds. Red stars indicate measurements taken after administering bupivacaine. The data show a large deviation in the peak response voltage in the three individual birds as well as a large deviation in the current threshold required to evoke a measureable response. This variability is most likely due to a combination of factors including the impedance of the integrated CNTf electrodes, variability in the oil insulation, or the amount of electrode material in contact with the nerve. Still, all data sets exhibit similar behavior in that the response voltage increases monotonically with increasing stimulation current.

4. Conclusions

In this study we have presented a novel micro-scale nerve cuff or ‘nanoclip’ electrode that is easy to implant and can perform recording and stimulation on small diameter nerves. The nanoclip addresses key challenges in interfacing with nerves in the peripheral nervous system, particularly for small animal pre-clinical models. We demonstrated the successful use of our nanoclip in the stimulation and monitoring of nerve activity in the TS nerve of the zebra finch. The subchronic safety of our nanoclip remains to be studied in detail through chronic histology, but is evidenced by the return of

birdsong structure to baseline after bilateral implants on the TS nerve. The nanoclip is fabricated using a flexible, high-resolution, direct-write laser printing technique. This fabrication paradigm provides for a rapid development cycle and the ability to create nanoclips of almost arbitrarily complex geometries. Expanding from the nanoclips shown here, many other designs can be envisioned containing electrode arrays of higher channel counts, distinct closure mechanisms, or even built from bio-degradable polymers (Applegate 2016).

For the carbon nanotube fiber electrodes presented here, the most pressing need is to develop methods of reliably insulating the CNTfs outside the clip, so that the device can be used without oil insulation—a key feature for future chronic applications in pre-clinical animal models. Figure 11 illustrates one possible path forward. Here, CNTfs were insulated with parylene (doped with the fluorescent molecule anthracene) and a two-photon scanning laser was used to selectively ablate the parylene over a length of 50–100 μm within the nanoclip. Using this process, a proof-of-principle device was constructed that could both stimulate and record evoked compound action potentials (figures 11(b) and (c)) in the absence of oil insulation. Additional tests are needed to determine the reliability of this fabrication process as well as the robustness of parylene-insulated CNTfs for use as chronic interconnects in the autonomic nervous system.

Acknowledgments

This work was supported by GlaxoSmithKline, the Welch Foundation (C-1668), the Air Force Office of Scientific Research (FA9550-15-1-0370), the Boston University Photonics Center, and the Boston University College of Engineering. The nanoclip has been described in a provisional patent filing (PR66142P US). The authors would also like to thank Dr Colin Young for his help with CNTf spinning.

References

Applegate M B *et al* 2016 Photocrosslinking of silk fibroin using riboflavin for ocular prostheses *Adv. Mater.* **28** 2417–20

Atwater J H *et al* 2011 Microphotonic parabolic light directors fabricated by two-photon lithography *Appl. Phys. Lett.* **99** 151113

Backris G L *et al* 2012 Baroreflex activation therapy provides durable benefit in patients with resistant hypertension: results of long-term follow-up in the Rheos Pivotal Trial *J. Am. Soc. Hypertens.* **6** 152–8

Behabtu N *et al* 2013 Strong, light, multifunctional fibers of carbon nanotubes with ultrahigh conductivity *Science* **339** 182–6

Bückmann T *et al* 2012 Tailored 3D mechanical metamaterials made by dip-in direct-laser-writing optical lithography *Adv. Mater.* **24** 2710–4

Bückmann T *et al* 2014 On three-dimensional dilational elastic metamaterials *New J. Phys.* **16** 033032

Conde S V *et al* 2014 Carotid body, insulin, and metabolic diseases: unraveling the links *Frontiers Physiol.* **5** 418

Delivopoulos E *et al* 2012 Concurrent recordings of bladder afferents from multiple nerves using a microfabricated PDMS microchannel electrode array *Lab Chip* **12** 2540–51

Famm K *et al* 2013 Drug discovery: a jump-start for electroceuticals *Nature* **496** 159–61

Hoppe U C *et al* 2012 Minimally invasive system for baroreflex activation therapy chronically lowers blood pressure with pacemaker-like safety profile: results from the Barostim neo trial *J. Am. Soc. Hypertens.* **6** 270–6

Hu C *et al* 2014 StyletChip: a microfluidic device for recording host invasion behavior and feeding of plant parasitic nematodes *Lab Chip* **14** 2447–55

Koopman F A *et al* 2016 Vagus nerve stimulation inhibits cytokine production and attenuates disease severity in rheumatoid arthritis *Proc. Natl Acad. Sci.* **113** 8284–9

Moore S K 2015 Follow the wandering nerve *IEEE Spectrum* **52** 78–82

Morris G L *et al* 2013 Evidence-based guideline update: Vagus nerve stimulation for the treatment of epilepsy report of the guideline development subcommittee of the American Academy of Neurology *Neurology* **81** 1453–9

Poole B, Markowitz J E and Gardner T J 2012 The song must go on: resilience of the songbird vocal motor pathway *PLoS One* **7** e38173

Sackeim H A *et al* 2001 Vagus nerve stimulation (VNS) for treatment-resistant depression: efficacy, side effects, and predictors of outcome *Neuropsychopharmacology* **25** 713–28

Tarver W and Cummins R 2006 Vagus nerve stimulation for the treatment of depression with therapeutically beneficial parameter settings *US Patent Specification* US 20060293721 A1

Vitale F *et al* 2015 Neural stimulation and recording with bidirectional, soft carbon nanotube fiber microelectrodes *ACS Nano* **9** 4465–74